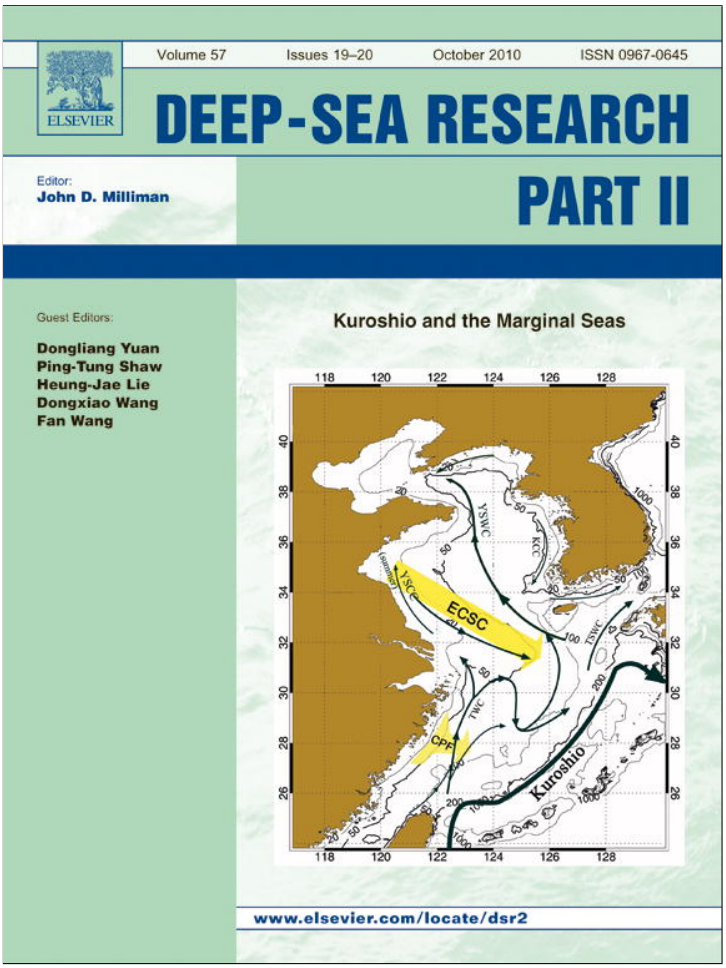

Deep-Sea Research II 57 (2010) 1809–1819

Contents lists available at ScienceDirect

Deep-Sea Research II

journal homepage: www.elsevier.com/locate/dsr2

Nutrient pumping/advection by propagating Rossby Waves in the Kuroshio Extension

Peter C. Chu*, Yu-Heng Kuo

Department of Oceanography, Naval Postgraduate School, Monterey, CA 93943, USA

ARTICLE INFO

Article history:
Received 22 April 2010
Accepted 22 April 2010
Available online 29 April 2010

Keywords:
Rossby wave propagation
Kuroshio extention
Nutrient pumping/advection
Meso-scale eddies
Sea level anomaly
Chlorophyll-a concentration

ABSTRACT

Ten years (1998–2007) of sea-level anomalies (SLA) from multiple satellite altimeters and chlorophyll-*a* concentration from the Sea-viewing Wide Field-of-view Sensor (SeaWiFS) were used to detect eddy pumping/advection of nutrients by the action of propagating Rossby waves in the Kuroshio Extension (KE) region near 35°N after the seasonal SeaWiFS chlorophyll-*a* (Chl-*a*) concentrations cycles and annual changes of altimeter SLA were eliminated. Spatial structure of Chl-*a* anomalies to the seasonal cycle is examined in relation to altimeter eddy structure. Eddy propagation speeds and scales by the Rossby waves are also identified. Chl-*a* structure is evident during the spring bloom period with a scale around 460 km. Cold-core (cyclonic) rings correspond to areas of high Chl-*a* concentrations. Warm-core (anticyclonic) rings relate to areas of low Chl-*a* concentration. Chl-*a* anomalies and SLA have an overall modest negative correlation coefficient of $r=-0.45$, which may imply the co-existence of both eddy pumping and eddy advection mechanisms in the KE region. Swirl currents between eddies redistribute surface chlorophyll concentrations and can spatially bias maximum and minimum concentration levels off eddy center. The correlation coefficient has seasonal fluctuations. In the western KE region, it varies from high negative correlation ($r=-0.70$) in April and September (eddy pumping dominant) to low negative correlation ($r=-0.33$) in February and March (eddy advection dominant). In the eastern KE region, it varies from high negative correlation ($r=-0.67$) in February to low negative correlation ($r=-0.42$) in December. It is noted that the characteristic wavelengths of the SLA and Chl-*a* features, and the seasonality of the correlation between these two variables have not been previously documented.

Published by Elsevier Ltd.

1. Introduction

Primary productivity in the open ocean is limited by the lack of nutrients in surface waters. These nutrients are mostly supplied from nutrient-rich subsurface waters through upwelling and vertical mixing (Barber, 1992). Vertical diffusivity was found to be related to primary production near the top of the Subtropical Mode Water (STMW) in the western North Pacific (Sukigara et al., 2009). Seasonal and intra-seasonal variability of SeaWiFS chlorophyll-*a* (Chl-*a*) in the North Pacific was identified using model and satellite data and the response of the biological production to the uplift and depression of the nutricline with the variability of mesoscale physical phenomena (Sasai et al., 2007). However, in the ocean gyres these mechanisms do not fully account for the observed productivity (Jenkins and Goldman, 1985). Various mechanisms have been proposed for explaining the primary productivity. Among them, upward pumping and horizontal advection of nutrients through the action of eddies are most popular. For example, upward pumping to account for the remainder of the primary productivity was identified from satellite data in regional seas such as Sargasso Sea (e.g., Siegel et al., 1999) and North Pacific Ocean (Uz et al., 2001). After analyzing the coherence between sea-level anomalies (SLA) and Chl-*a* from satellite data, Uz et al. (2001) claimed the importance of pumping mechanism with westward propagating Rossby waves for the Chl-*a* structure. Chu and Fang (2003) also detected the Rossby wave propagation in the South China Sea from satellite altimetry data. The eddy swirl currents also advect phytoplankton concentrations at rates less, comparable or greater than the propagation rates of concentration structures due to phytoplankton growth dynamics. At external regions, chlorophyll structure can be moved between eddies and so chlorophyll can be mixed across concentration gradients (Leterme and Pingree, 2008).

Thus, two competing mechanisms, eddy pumping and eddy advection, co-exist. The eddy pumping mechanism causes high Chl-*a* concentration anomaly co-located with the cyclonic eddy; and low Chl-*a* concentration anomaly is co-located with the anticyclonic eddy. The eddy advection mechanism causes mixing

* Corresponding author.
E-mail address: pcchu@nps.edu (P.C. Chu).

0967-0645/$ - see front matter Published by Elsevier Ltd.
doi:10.1016/j.dsr2.2010.04.007

between high- and low-Chl-*a* regions. If the pumping mechanism dominates, the negative correlation between SLA and Chl-*a* concentration anomaly is high. If advection mechanism dominates, the negative correlation between SLA and Chl-*a* concentration anomaly is low.

In this study, 10 years (1998–2007) of SLA from multiple satellite altimeters and Chl-*a* concentration from the Sea-viewing Wide Field-of-view Sensor (SeaWiFS) were used to detect eddy pumping/eddy advection of nutrients by the action of propagating 2.

2. Kuroshio Extension

The Oyashio Current water is formed by East Kamchatka Current water and Okhotsk Sea water modified by mixing in the Kuril straits. It flows southwestward along the Kuril Islands and turns eastward from the northern coast of Japan. The Kuroshio flows northward from the tropical area to Tohoku area east of Japan. The Kuroshio turns eastward from the eastern coast of Honshu, Japan, and the strong eastward flow around 35°N is called the KE (mid-latitude western boundary current outflow region), which is the continuation of the warm, northward-flowing waters of the Kuroshio western boundary current, and forms a vigorously meandering boundary between the warm subtropical and cold northern waters of the Pacific. The warm Kuroshio waters encounter the cold dry air masses coming from the Asian continent, and create intense air sea heat exchanges in the KE region. Solomon (1978) discovered a current ring detached from the large quasi-steady Kuroshio meander south of Honshu in May 1977. The ring remained stationary until August, when it recombined with the main Kuroshio to reform a meander distorted in shape and upstream from the original meander. Meanders which separate northward of the KE jet generate anticyclonic (warm-core) eddies and those which separate southward of the KE jet produce cyclonic (cold-core) eddies. The warm-core eddies on the northern side are originated mostly from the area of Sanriku, and the cold-core eddies on the southern side are mainly generated from the area off the Boso Peninsula (Sun et al., 1989). A complete life history of cyclonic ring was observed: a southward meander of the KE jet, its pinching-off to form a cyclonic ring, the ring's westward movement, its coalescence with the KE jet (Ichikawa and Imawaki, 1994).

Fig. 1 shows two quasi-stationary meanders with their ridges located at 144 and 150°E exist along the mean path of the upstream KE (Qiu and Chen, 2005). A tight recirculation gyre is located south of the quasi-stationary meanders of the KE jet, and increases the eastward transport of the KE from near 50 Sv to about 130 Sv (where 1 Sv$=10^6$ m^3 s^{-1}). Near 159°E, the KE jet encounters the Shatsky Rise where it often bifurcates: the main body of the jet continues eastward, and a secondary branch tends to move northeastward to 40°N where it joins the Subarctic Current (e.g., Mizuno and White, 1983; Niiler et al., 2003). With the broadening in its width downstream of 160°E, the KE loses its inertial jet characteristics and rejoins gradually the interior Sverdrup circulation as the North Pacific Current.

Remotely sensed data collected since the late 1970s provides oceanographers with a large volume of information on the state of the surface of the World Ocean. Qiu and Chen (2005) analyzed twelve years of SLA from multiple satellite altimeters. In the KE region, part of SLA measured by the altimeters reflects the seasonally varying surface heat flux that causes expansion or contraction of the water column (e.g., Stammer, 1997; Gilson et al., 1998). Qiu and Chen (2005) removed these steric height changes from the weekly SLA dataset and investigated the low-frequency changes and the interconnections of the KE jet, its southern recirculation gyre, and their mesoscale eddy field. Following Qiu and Chen (2005), the axis of the KE jet is defined by the 170-cm sea surface height contours, which are consistently located at, or near, the maximum of its latitudinal gradient (Fig. 2).

3. Methods and data

3.1. SLA

SLA heights have been measured by the ERS 1/2 and TOPEX/Poseidon satellites from 1 January 1998 to 31 December 2007 at 7-day intervals. Radar altimeters on board the satellite continually transmit signals at high frequencies to Earth and receive reflected signals from the sea surface. The data have been

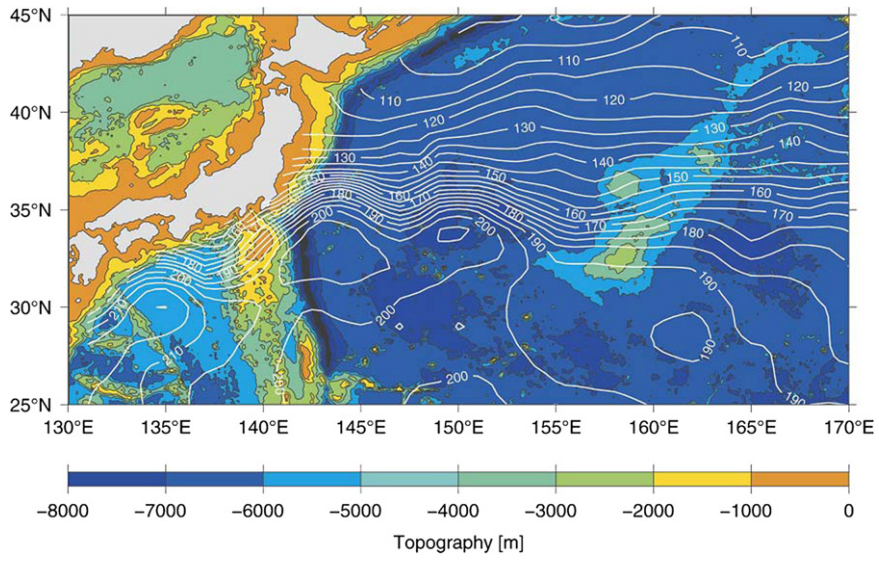

Fig. 1. Surface dynamic height field (cm; white contours) relative to 1000 dbar from Teague et al. (1990). Colored map shows the bathymetry based on Smith and Sandwell (1994). Major bathymetric features in the region include the Izu–Ogasawara Ridge along 6.40°E and the Shatsky Rise around 159°E (after Qiu and Chen 2005).

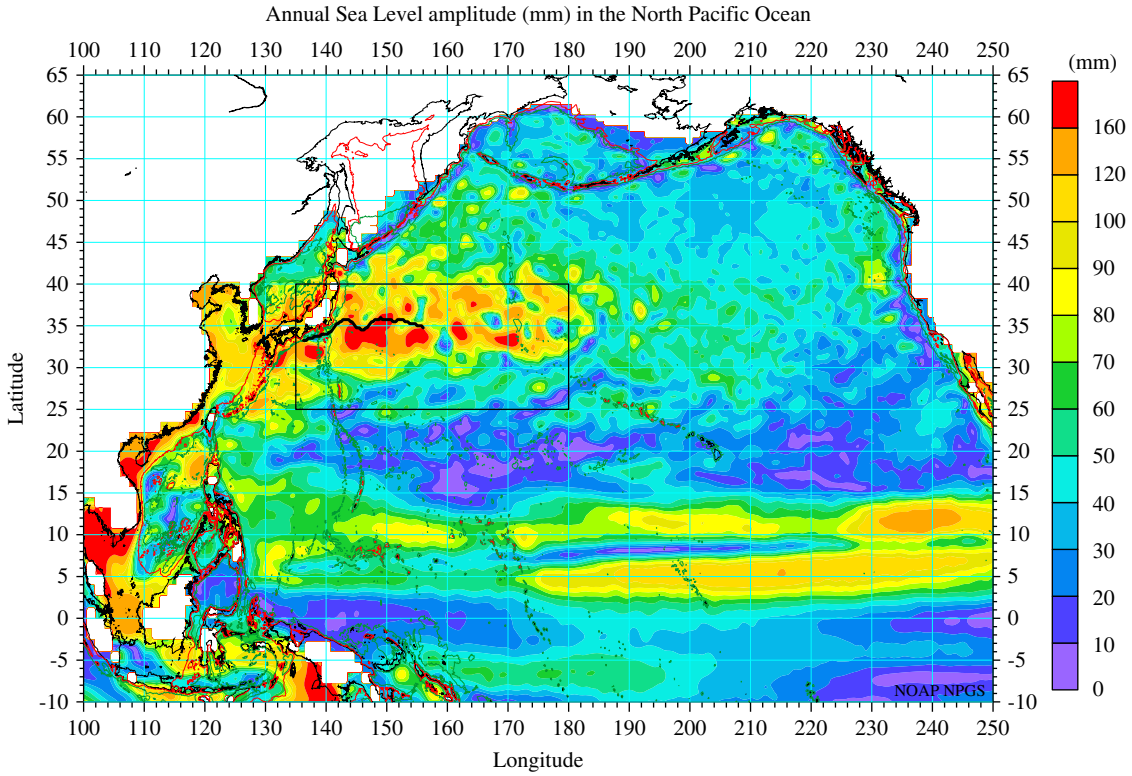

Fig. 2. Annual sea-level amplitude (mm) in the North Pacific Ocean. The Kuroshio Extension route selected (marked blank) along the 170 cm SSH contour (see Fig. 1), which is associated with large amplitude region.

processed according to Le Traon et al. (1998) with SLA spatially interpolated to 0.25° in both latitude and longitude. Maps of SLA were derived for the North Pacific to compare with monthly composites of Chl-*a* concentration.

SLA has evident annual cycle and mesoscale structure dominated by eddy or Rossby waves. The annual signal is influenced partially by the ocean circulation and partially by the rise and fall of the sea surface that arises from the expansion and contraction of the ocean due to its heating and cooling with seasonal change. The region of large variance of sea-surface height in the North Pacific is along the mean KE jet (represented by 170-cm contour in Fig. 1), where the annual buoyancy and recirculation changes cause a maximum annual elevation change of about ± 20 cm (Fig. 2). Since we are interested in elevation structure that correlates with non-seasonal Chl-*a* structure, the annual component and any residual mean elevation removed from the SLA data using the Fourier analysis. Although relatively small in this context, aliasing due to the semi-diurnal tide is also removed. We refer to the resulting data as SLA residuals. The mean KE jet selected is a few degrees north of the maximum annual amplitude of SLA (Fig. 2) and other spectral components tended to show similar distributions of amplitude structure.

Altimeter and Chl-*a* data are also extracted every 0.25° along the mean KE axis (corresponding to 80 stations sampled over a distance of 1820 km; Fig. 3) from January 1998 to December 2007 (10-year period). Temporal variations of sea-surface elevation residuals and Chl-*a* along the mean KE axis are plotted on time-longitude cross-sections. An overlapping time window of Chl-*a* anomalies and altimeter residuals is compared.

3.2. Chl-a

Chl-*a* data were obtained from the Goddard Distributed Active Archive Center under the auspices of NASA. Use of these data is in accordance with the SeaWiFS Research Data User Terms and Conditions Agreement. The SeaDAS software was used to compute Chl-*a* concentration (C_a) from the ratio of radiances measured in band-3 (480–500 nm) and band-5 (545–565 nm) according to the following NASA algorithm,

$$C_a = \exp[0.464 - 1.989\,\mathrm{Ln}(L_{WM}490/L_{WM}555)], \quad (1)$$

and monthly composite Chl-*a* maps for the North Pacific were derived. For deriving the 10-year mean seasonal cycles, the Chl-*a* data are spatially averaged over ± 25 km in both latitude and longitude and missing data due to cloud coverage interpolated. For example, Fig. 4 shows the Chl-*a* structure and SLA residual in April 2007. The velocities were determined using the geostrophic relation from SLA residual map (Fig. 4B). To examine the eddy effect on Chl-*a* structure, seasonal cycles were removed from the Chl-*a* and SLA data. The Chl-*a* anomalies or residuals were compared to the SLA residuals from January 1998 to December 2007.

4. Results

4.1. Structure of Chl-a and SLA

The Chl-*a* monthly composite for April 2007 shows the spring bloom boundary arbitrarily defined by concentration levels of 0.2 mg m^{-3} Chl-*a* concentrations (Fig. 4A). The boundary is not regular but has perturbations due to eddy structure. The North Pacific SLA map for April 2007 (Fig.4B) shows the corresponding mesoscale eddy field. The main open-ocean dynamical influences on the Chl-*a* field are vertical pumping and/or horizontal advection by eddies with a length scale around 460 km.

To identify the association between spatial patterns of eddy and Chl-*a* concentrations for the KE extension area (rectangular box in Fig. 4), we re-plot Chl-*a* concentrations (in color) and SLA

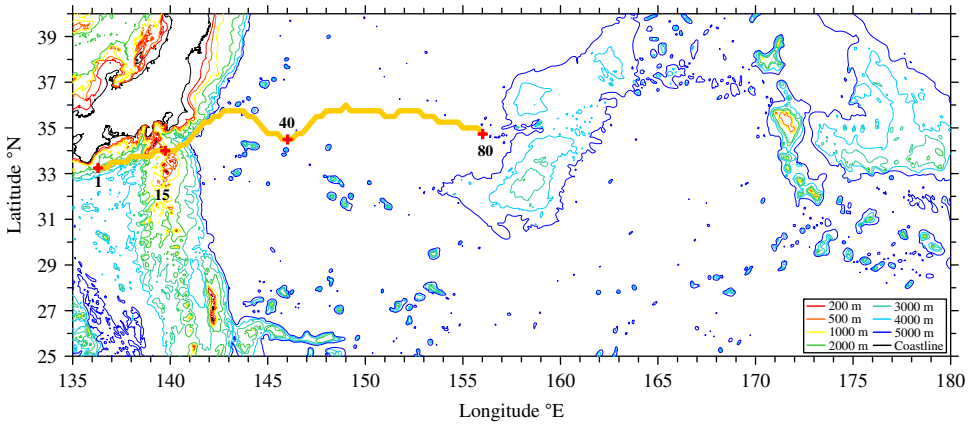

Fig. 3. Topography of the studied area and Kuroshio Extension axis (marked orange) adopted for the present study. Stations positions 1, 15, 40 and 80 are marked.

(in contour) in Fig. 5. High SLA values (anticyclonic eddies) are indicated by capital letters (A, B, C, D, E, F, G, H), and low SLA values (cyclonic eddies) are marked as numerical numbers (1, 2, 3,…). Cyclonic (anticyclonic) eddies are co-located with high (low) Chl-a concentration areas.

At Station-1 (136.25°E, 33.25°N) (see Fig. 3), the beginning of the KE jet, Chl-*a* concentratiosn have an evident seasonal cycle with a strong spring bloom (March-April) and a weak fall bloom (Fig. 6) with a maximum Chl-*a* concentration of 0.97 mg m^{-3} in April 2000 and a minimum Chl-*a* concentration of 0.12 mg m^{-3} in September 2007. Chl-*a* concentrations start to increase in the winter period (after September) as the mixed layer deepens due to winter mixing (with nutrient renewal). The sea-surface temperature (SST) on the KE Observatory mooring site nominally at 32.4°N, 144.6°E (see website: http://www.pmel.noaa.gov/keo/data.html) shows that the bloom maximum occurred in April (see Fig. 9) early during the development of the seasonal thermocline. The combination of modest stratification and nutrients left over from the winter mixing allows rapid phytoplankton growth near the surface.

4.2. Fluctuations of Chl-a and SLA along the mean KE jet axis

Inspection of both SLA and Chl-*a* maps show more intense spatial structure in the KE region. Mean and variance of Chl-*a* concentrations (Fig. 7) and variance of SLA (Fig. 8) are calculated at all stations (1–80) nearly 0.25° apart along the mean KE jet axis. There is a significant difference in Chl-*a* concentrations between stations 1 and 15 and stations 16 and 80. The mean Chl-*a* concentration is estimated as

$$\overline{x}_{\mathrm{Chl}\,a} \pm \sigma = 0.37 \pm 0.02 \text{ mg m}^{-3} \quad (2)$$

for stations 1 to 15, which is higher than

$$\overline{x}_{\mathrm{Chl}a} \pm \sigma = 0.28 \pm 0.02 \text{ mg m}^{-3} \quad (3)$$

for stations 16 to 80. The difference in Chl-*a* is likely due to the changing properties along the mean KE axis. Between stations 1 and 15, at the beginning of the KE jet, the water is more in the proximity of the coast that leads to greater nutrient fluxes to the euphotic zone. The monthly distribution maps show that high Chl-*a* inflow off Japan coast is most evident in April (see Fig. 5). The SLA shows high fluctuations in variance along the KE axis (Fig. 8),

$$\sigma^2_{\mathrm{SLA}} = 870 \pm 460 \text{ cm}^2. \quad (4)$$

The maximum variance of 1800 cm^2 corresponds to a root mean squared fluctuation of sea level of about ± 42 cm on the mean KE jet axis. The SLA variance increases generally from 186 cm^2 at Station-1 (33.25°N, 136.25°E) to near 1770 cm^2 at Station-36 (34.75°N, 145°E). Small SLA variance values might represent a regular pattern of nodes or a meander scale extending 600 km from the position where the KE jet leaves Japanese coast.

4.3. Two seasonal blooms in the KE region

Chl-*a* structure in space and time may be masked by a dominant seasonal cycle so the Chl-*a* anomalies or residuals are defined as differences from a mean seasonal cycle. The seasonal cycles obtained for stations 1 to 15 (horizontal scale ~ 500 km) and stations 16 to 80 (horizontal scale ~1500 km) are shown in Fig. 9. Two peaks in the annual Chl-*a* cycle, spring and fall blooms are mainly determined by light and nutrient limitation, respectively. Just below a euphotic layer the concentration of nutrients increase with depth. On such large horizontal scales, vertical stability is a major factor to affect the nutrient limitation and vertical position of phytoplankton (two opposite effects on phytoplankton concentration). Usually, strong (weak) vertical stability reduces (increases) the nutrient supply and allows (disallows) phytoplankton to stay in the euphotic layer. In winter (December-February), the ocean surface mixed layer is deep. Weak vertical stability does not allow phytoplankton to stay in the euphotic layer, which causes low production (low values of Chl-*a* in Fig. 9) since phytoplankton cannot obtain light enough for growth even with a high nutrient supply. As spring approaches, vertical stability strengthens; phytoplankton can stay in the euphotic layer long enough to grow with reduced (but sufficient) nutrient supply from the winter, so that a spring bloom starts and reaches maximum production in April (0.55 mg m^{-3} Chl-*a*). In summer (June - August), the water column is too stable. Strong vertical stability limits the nutrient supply from deep water, which causes low production with a minimum value in August (0.25 mg m^{-3} Chl-*a* for stations between 1 and 15, and 0.15 mg m^{-3} Chl-*a* for stations between 16 and 80), since phytoplankton cannot get sufficient nutrients even staying the euphotic layer. As fall approaches, the vertical stability weakens; supply of nutrients from deep water increases. Phytoplankton is still within the euphotic layer. This leads to a second bloom in November (0.43 mg m^{-3} Chl-*a* for stations between 1 and 15, and 0.30 mg m^{-3} Chl-*a* for stations between 16 and 80). Thus, the spring bloom results from increased light levels and the autumn bloom are a response to nutrient availability due to increased vertical mixing and seasonal thermocline erosion.

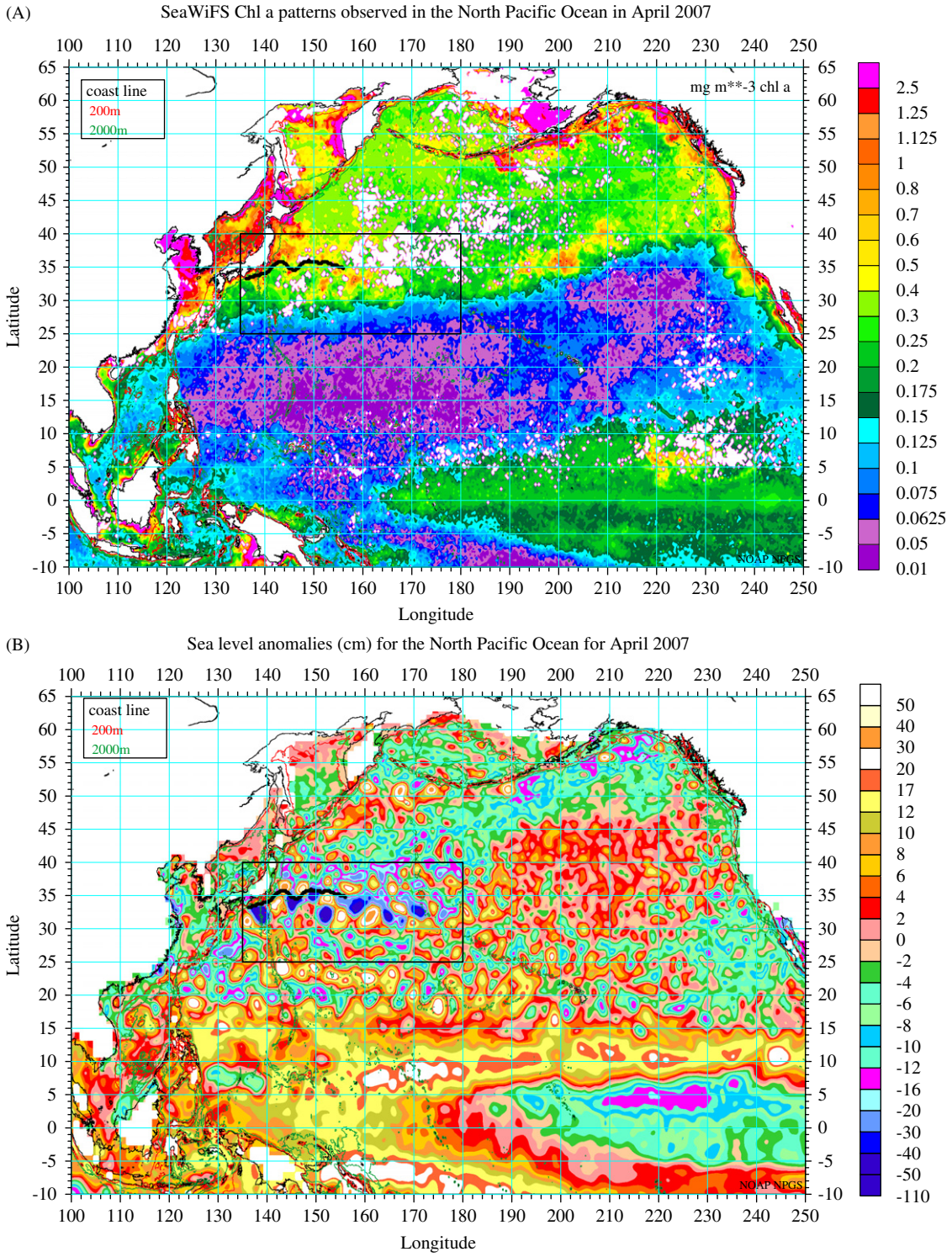

Fig. 4. Satellite observed (A) Chl-*a* concentrations (mg/m^3) and (B) sea-level anomalies (cm) in the North Pacific in April 2007. Kuroshio Extension route is represented by a thick black curve in Fig. 4A.

4.4. *Propagation of eddies by Rossby waves*

The SLA residuals have the local annual component removed and the mean value at a point is zero. Intense mesoscale activity, warm-core rings (yellow/red) and cold-core rings (blue), can be identified along the mean KE jet axis (Fig. 10). The propagation of these rings over the time varies according to their location. Many eddies are identified. We chose two anticyclonic eddies (a and b) and two cyclonic eddies (c and d) (Fig. 10) for illustration. They were all propagating westward in the path of the KE jet with an average speed of 3.05–4.92 km day^{-1} (A and B) and 1.16 km day^{-1} (1 and 2). These eddies exist at least for six months.

A scale, *L*, for eddies or rings on the KE jet axis was estimated by measuring the separation distance between positive or negative anomalies along the eastern half of the axis where the

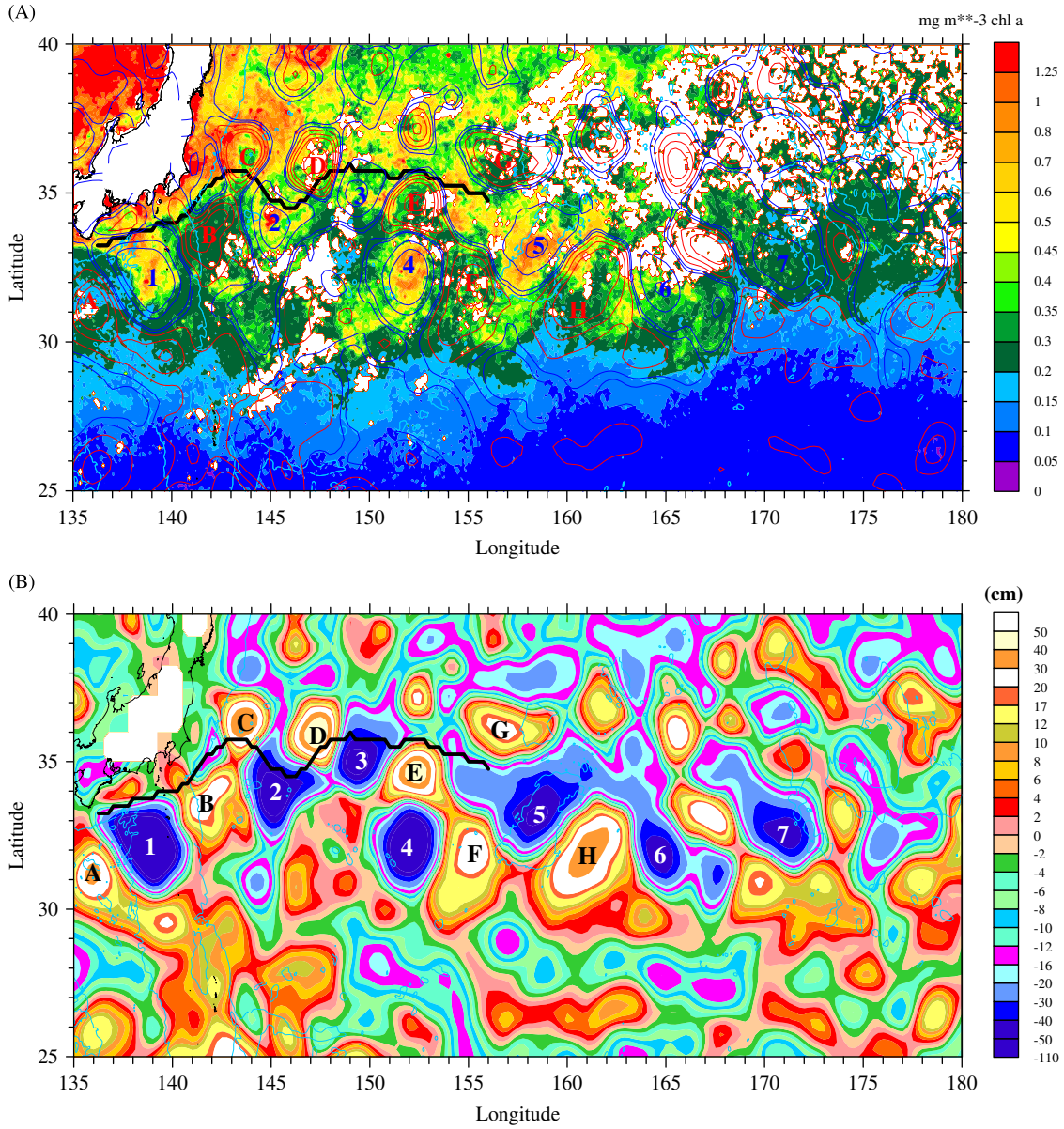

Fig. 5. (A) Chl-*a* concentration color plot in conjunction with SLA (cm) contour, and (B) SLA color plot for the Kuroshio Extension area (25°N–40°N, 136°E–180°E) in April 2007 . The mean KE jet axis is represented by the thick black curve. Anticyclonic eddies (high SLA) are marked by capital letters (A, B, C, D, E, F, G, H) and cyclonic eddies (Low SLA) are marked by numbers (1, 2, 3,…).

anomaly structures were more marked. A separation or anomaly wavelength was determined as

$$L = 460 \pm 65 \text{ km} \quad (5)$$

from Fig. 10, but extended for a 10-year period.

4.5. Eddy pumping and eddy advection mechanisms

Removing the mean Chl-*a* seasonal cycle from the SeaWiFS data for stations 1–80 gives the Chl-*a* anomaly time series along the mean KE jet axis (Fig. 11). Warm-core (anticyclonic) rings generally correspond to areas of low Chl-*a* concentration. For example, the anticyclonic eddies marked a and b (Fig. 9) corresponds to the low Chl-*a* pattern (Fig. 11). Cold-core cyclonic eddies marked c and d (Fig. 10) corresponds to high level Chl-*a* pattern (Fig. 11). Other lower SLA residuals (marked - in Fig. 10) are associated with higher Chl-*a* values (marked + in Fig. 11) and vice versa. The linear regression equation between Chl-*a* (mg m^{-3}) and SLA (cm) anomalies is given by

$$\text{Chl-}a = -0.0169\text{SLA}, \quad (6)$$

for Stations 1–15, and

$$\text{Chl-}a = -0.0111\text{SLA}, \quad (7)$$

for Stations 16–80. It shows that the Chl-*a* scale or anomaly wavelength along the KE jet axis will match the separation scale between SLA residuals or eddies of the same sign. However, the Chl-*a* structure (Fig. 11) was too fragmented for an estimate of scale along the KE jet axis. Instead, a wavelength value was determined from monthly Chl-*a* concentration maps for occasions when alternating positive/negative concentration anomaly was evident along the KE route. This method gave an independent value of $L = 460 \pm 65$ km, based on monthly occurrences when there was a tendency for a repeating structure or oscillation wavelength along the KE route (see Fig. 5, for example). The more

regular Chl-*a* structure could be matched (in position and time) with negative SLA anomalies on SLA maps.

In the central region of an eddy, the eddy currents move with the eddy and so just turn the chlorophyll structure at near constant radius within the eddy. At external regions, chlorophyll structure can be moved between eddies and so chlorophyll can be mixed across concentration gradients. For eddy currents, to show a significant redistribution of a phytoplankton bloom, the eddy swirl currents must be able to advect phytoplankton concentrations at rates comparable or greater than the rates of change of concentration due to phytoplankton growth dynamics. Besides, the swirl currents can cause enhanced gradients in chlorophyll with some re-distribution related to lateral diffusion. Because the length scales are relatively large, in most geophysical flows lateral diffusion is rarely significant compared with the vertical diffusion. Instead, the secondary circulations at fronts caused by these swirl currents are doing the bulk of the lateral transports relative to the mean flow on the scale of the eddies.

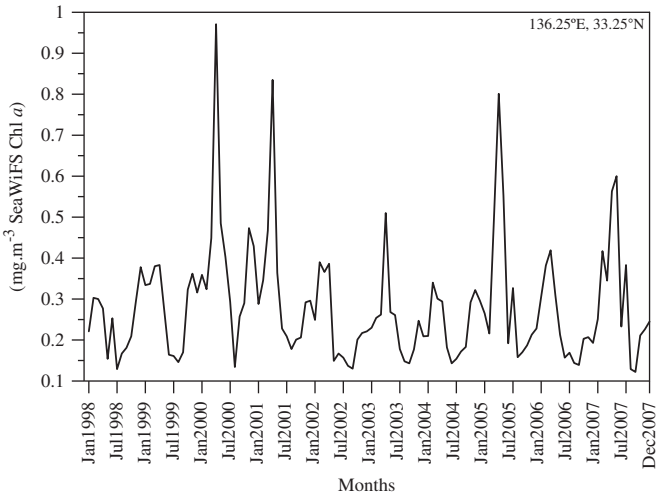

Fig. 6. Temporal variation of Chl-*a* concentrations (mg m^{-3} Chl *a*) at 136.25°E, 33.25°N.

The relationship between Chl-*a* and SLA residuals is analyzed for the two different water masses sampled along the route. Usually, strong (weak) negative correlation may imply the dominance of eddy pumping (eddy advection) mechanism. A negative correlation is found for the Subtropical Water, for Stations 1 and 15 ($r=-0.45$, $p<0.001$; Fig. 12A) and for the other part of the route, Stations 16 to 80 ($r=-0.43$, $p<0.001$; Fig. 12B). The overall modest negative correlation for Stations 1–80 (Fig. 10) ($r=-0.45$, $p<0.001$) suggests the co-existence of eddy pumping and eddy advection mechanisms in the KE region.

Such negative correlations have different seasonal variations (Fig. 13) between two parts along the KE axis especially for Stations 1–15. A maximum negative correlation occurs in September ($r\sim-0.70$) (eddy pumping dominance), and a minimum negative correlation occurs in February ($r\sim-0.33$) (eddy advection dominance). For Stations 16–80, such a seasonal variation is not evident.

4.6. Eddy swirl velocity

The velocity of tangential flow due to eddies can be determined by applying the geostrophic relation to maps of SLA (e.g. Figs. 4B and 5):

$$\frac{v^2}{R}+fv=-g\frac{\Delta\eta}{\Delta n}, \tag{8}$$

where f is the Coriolis parameter; η is SLA; v is the horizontal tangential swirl velocity; R is the radius of curvature of the eddy; g is the gravitational acceleration; and $\Delta\eta$ is the elevation change over a distance Δn in the normal direction of eddies. Applying Eq. (9) to eddies B/C or E/F (see Fig. 5) and neglecting the curvature term (v^2/R) give maximum speeds between eddies of

$$v\approx\frac{g}{f}\frac{d\eta}{dx}\sim 0.57\ \mathrm{m\ s^{-1}}. \tag{9}$$

In the KE region, chlorophyll levels are elevated towards the slope and shelf region and eddy currents could produce curved chlorophyll plume structures of a few hundred kilometers in a several days. For eddies, to be able to produce the chlorophyll structures a, b, c, d and e (see Fig. 5) along the spring bloom

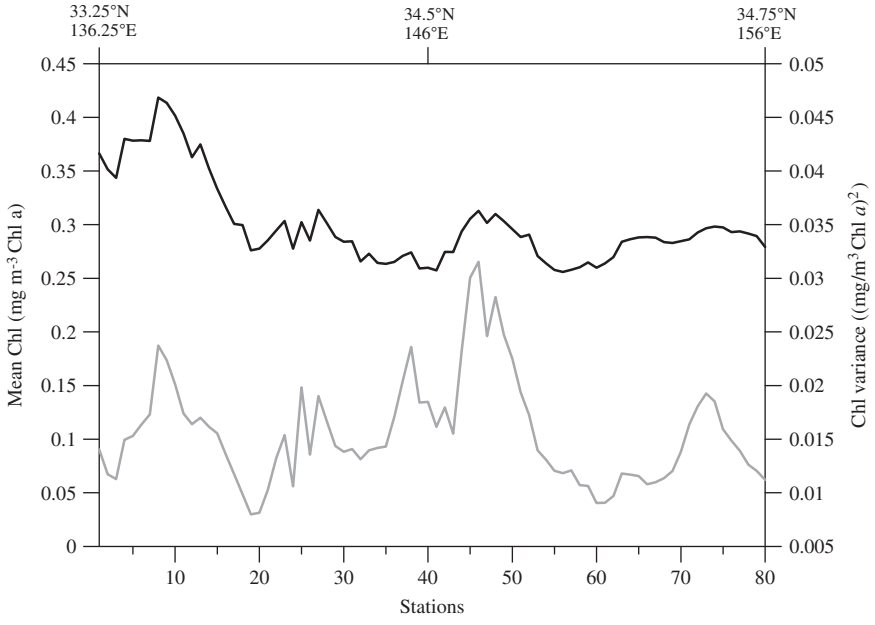

Fig. 7. Mean of Chl-*a* (mg m^{-3} Chl-*a*; black curve) and variance (seasonal cycle removed) of Chl-*a* ([mg m^{-3} Chl *a*]^2; grey curve) along the route of the Kuroshio Extension for a 10 years period (1998–2007).

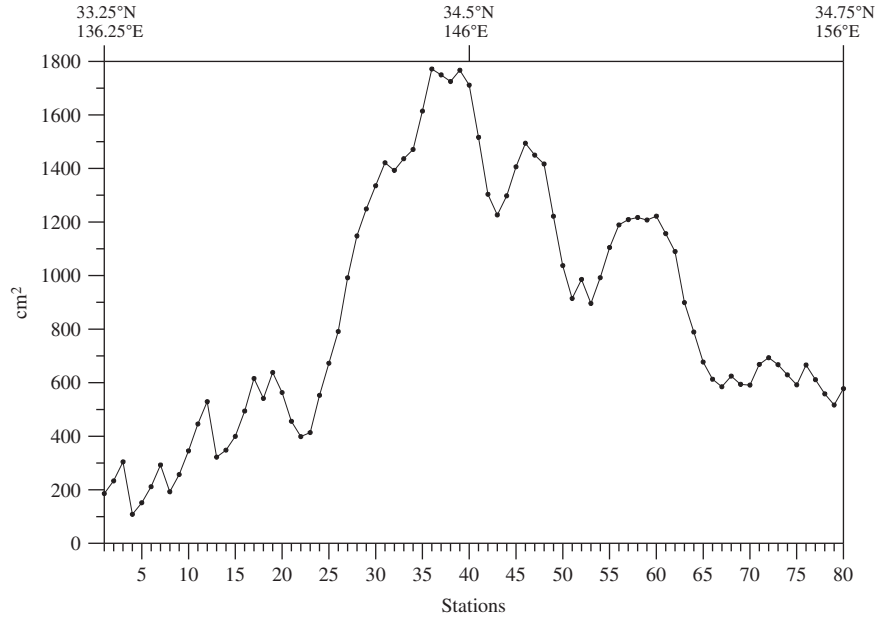

Fig. 8. Variance (annual component removed) of sea-level anomalies (cm^2) along the route of the Kuroshio Extension for a 10 years period.

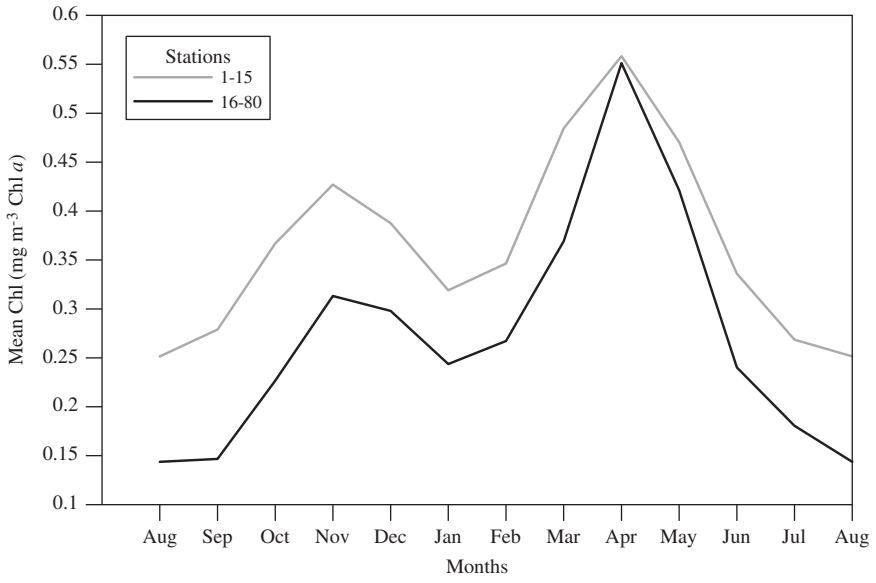

Fig. 9. Chl-*a* (mg m^{-3} Chl *a*) seasonal cycle along the route of the Kuroshio Extension. The results for station 1–15 are in grey and for station 16–80 in black.

frontal boundary, it is necessary to show that the eddy current structure can result in southward flow speeds that are as fast or faster than the northward propagation speed of the chlorophyll structure such as Chl-*a* plume c on the western side of cyclonic eddy 1 identified by SLA structure (Fig. 5A).

5. Discussion and conclusions

The Kuroshio Extension current represents the boundary between Subtropical Water (i.e. with high dynamic heights) and Slope and Subpolar Waters (i.e. with low dynamic heights) and sea-elevation changes or SLA variance levels are a maximum as eddies and meanders cross a mean route. This boundary in terms of Chl-*a* levels (lower and elevated Chl-*a* levels) is south of the KE jet. Kuroshio Extension meanders and rings carry different water types across a mean Kuroshio Extension jet position.

Two seasonal blooms are identified from 10 years (1998–2007) of SeaWiFS data. The major bloom is in April (spring bloom) with a maximum Chl-a concentration of 0.55 mg m^{-3}. The second bloom is in November (fall bloom) with a maximum Chl-a concentration of 0.43 mg m^{-3} for stations 1 and 15, and 0.30 mg m^{-3} for stations between 16 and 80. The low productivity in winter (December-February) is mainly caused by weak vertical stability and a deep mixed layer resulting in the phytoplankton being light limited. In spring phytoplankton is trapped in the euphotic layer long enough due to strengthened vertical stability to grow with reduced (but sufficient) nutrient supply from the winter. Nutrient concentrations and light are both sufficient for a secondary phytoplankton bloom.

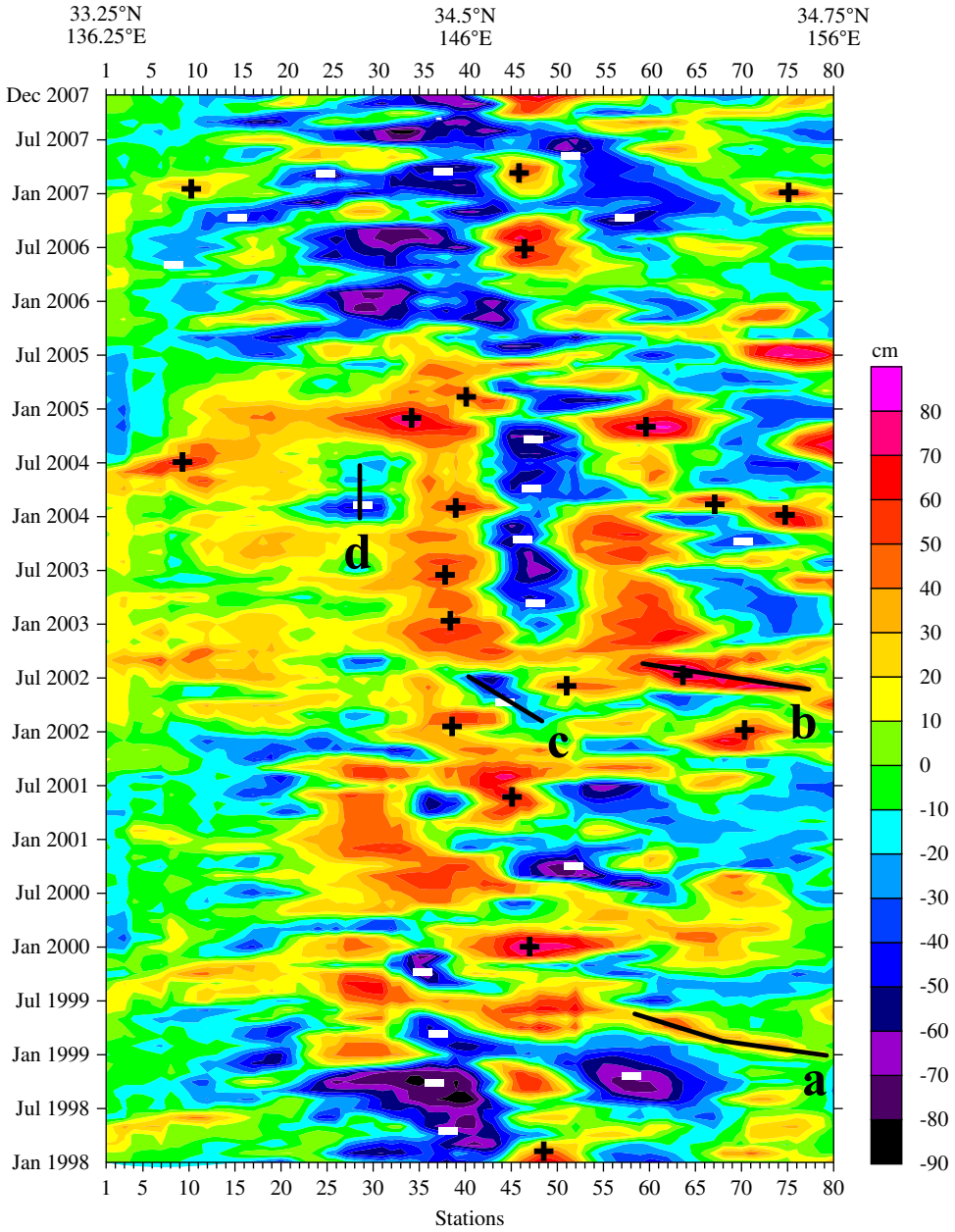

Fig. 10. Time-longitude cross-section of SLA residuals along the route of the Kuroshio Extension between January 1998 and December 2007. The altimeter signal is the SLA (cm) with the annual signal removed. Anticyclonic (a, b) and cyclonic (c, d) eddies have been followed in time and space. Negative sign indicates position of a low SLA associated with elevated Chl-*a* anomaly (+ in Fig. 11). Positive sign indicates position of a high SLA associated with lower Chl a anomalies (− in Fig. 11).

Cyclonic (cold-core ring) and anticyclonic (warm-core ring) eddies in the Kuroshio Extension region could propagate westward, could exist for at least six months or more, and could exhibit a zonal ocean color signal (SeaWiFS). A wavelength scale from one cold ring to another along the axis of the Kuroshio Extension jet was determined as 460 km. The rings have shown two distinct types of movement. Both anticyclonic and cyclonic rings have been observed moving upstream. Several warm-core rings can be found moving westward in the Slope Water with speeds between 3.5–5.7 cm s^{-1}. Cold-core rings well separated from the Kuroshio Extension generally move westward at about 1.4 cm s^{-1}.

Chlorophyll-*a* concentration is redistributed at the eddy scale mainly by the eddy pumping and affected by the horizontal advection due to surface swirl currents. The co-existence of eddy pumping and eddy advection mechanisms is identified by an overall modest negative correlation coefficient ($r=-0.45$) between Chl-*a* concentration and SLA residuals along the selected Kuroshio Extension axis. The Chl-*a* spatial variation or meander wavelength was about 460 ± 65 km and equal to the altimeter SLA separation determined between cold-core or warm-core rings along the route.

The eddy pumping mechanism is illustrated as follows. In general, the positive elevations anomalies are low in chlorophyll with a core of Subtropical Water. Seven anticyclones can be seen in Fig. 5A. All these anticyclonic eddies near the Kuroshio Extension axis have low chlorophyll concentration (labeled A–H, Fig. 5A). Anticyclonic eddies are associated with depressed isotherms with low levels of inorganic nutrients. Along the Kuroshio Extension, lower chlorophyll-*a* residual (marked with

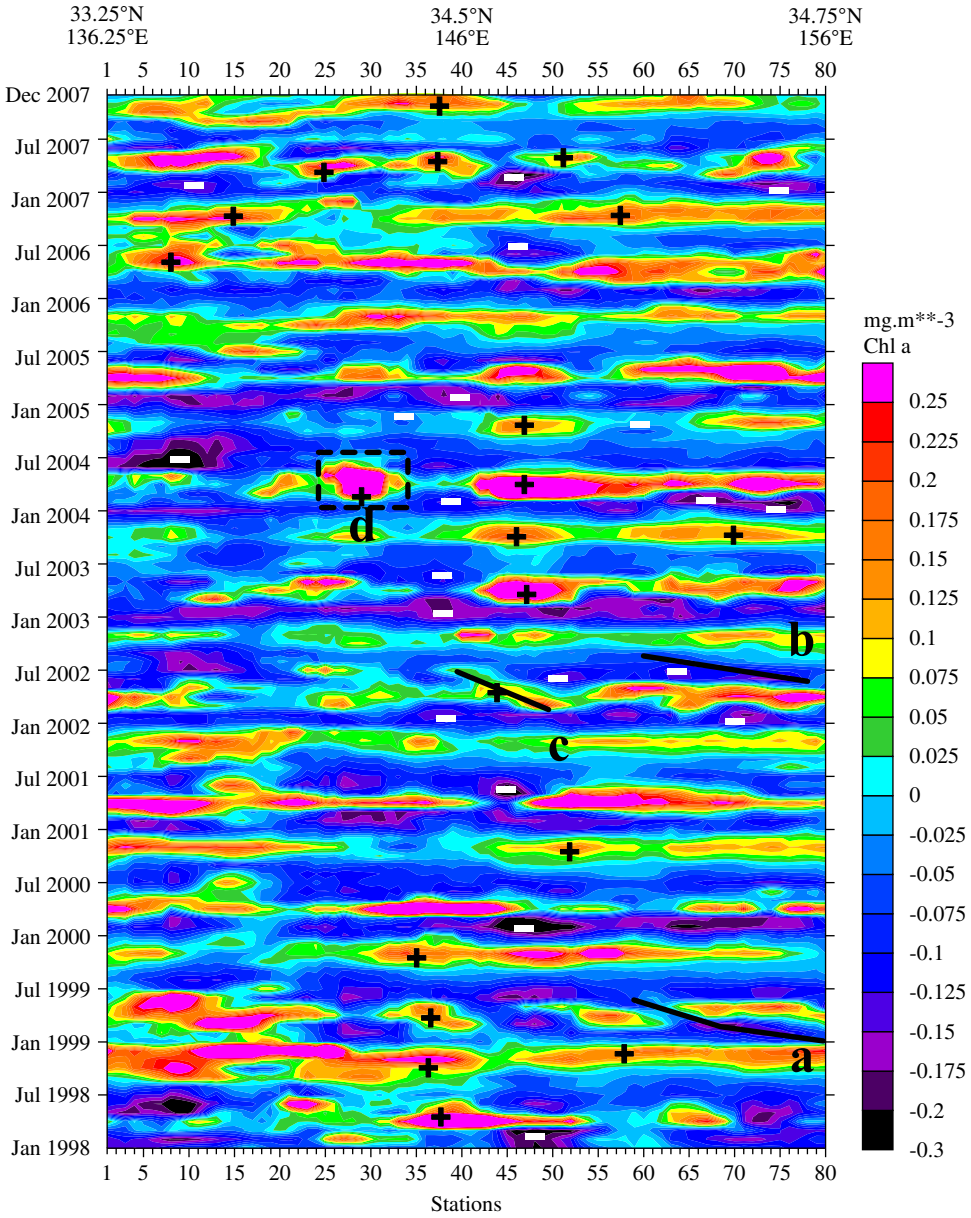

Fig. 11. Time-longitude cross-section of Chl-*a* residuals along the route of the Kuroshio Extension between January 1998 and December 2007. The Chl-*a* signal is the SeaWiFS Chl-*a* (mg m^{-3}) with the seasonal cycle removed. The high Chl-*a* (c, d) correspond to cyclonic eddies (C, D, Fig. 10) and the low Chl-*a* (a, b) correspond to anticyclonic eddies (A, B, Fig. 10). Positive sign indicates position of elevated Chl-*a* anomalies associated with low SLA (− in Fig. 10). Negative sign indicates position of lower Chl-*a* anomalies associated with high SLA (+ in Fig. 10).

− sign, Fig. 11) occur with positive SLA or anticyclonic structure (marked with + sign, Fig. 10). Cyclonic eddies have higher levels of inorganic nutrients, the isotherms are domed upwards (eddy pumping) and localized upwelling or mixing may introduce new nutrients into the euphotic zone, which could cause higher primary production in their core (Hitchcock et al., 1993; Arístegui et al., 1997). Cold core rings are thus generally higher in Chl-*a* and cyclonic rings marked 1, 2, 3, 4 south of the Kuroshio Extension axis have elevated chlorophyll concentrations (Fig. 5A). The ring or eddy currents may also redistribute the surface Chl-*a* levels, drawing out plumes of locally increased Chl-*a* from regions of higher Chl-*a*. This effect can be seen in some SLA maps and SeaWiFS monthly composites, April 2007 (Fig. 5), for example, where the eddy current structure draws out plumes (Fig. 5, near anticyclonic ring E, or around cyclone 4, for example) and in the time-longitude cross-sections (Figs. 9 and 11). From February to July 2001 and from stations 48 to 40 there is negative SLA anomaly (marked C, Fig. 10). Near the same area and for the same period, a SeaWiFS positive anomaly can be observed in Fig. 11 (labeled c).

The negative correlation between Chl-*a* concentration and SLA residuals has seasonal variability ($-0.70 < r < -0.33$). This reflects change of relative importance of the eddy advection mechanism versus eddy pumping mechanism. The strong negative correlation (such as $r = -0.70$ in April and September for Stations 1–15) indicates the dominance of eddy pumping mechanism. The weak negative correlation (such as $r = -0.33$ in February for Stations 1–15) indicates the dominance of the eddy advection mechanism.

Finally, it is noted that SeaWiFS provides an estimate of only near-surface chlorophyll concentrations. Especially in the sub-tropical western Pacific it appears that there are often sub-surface

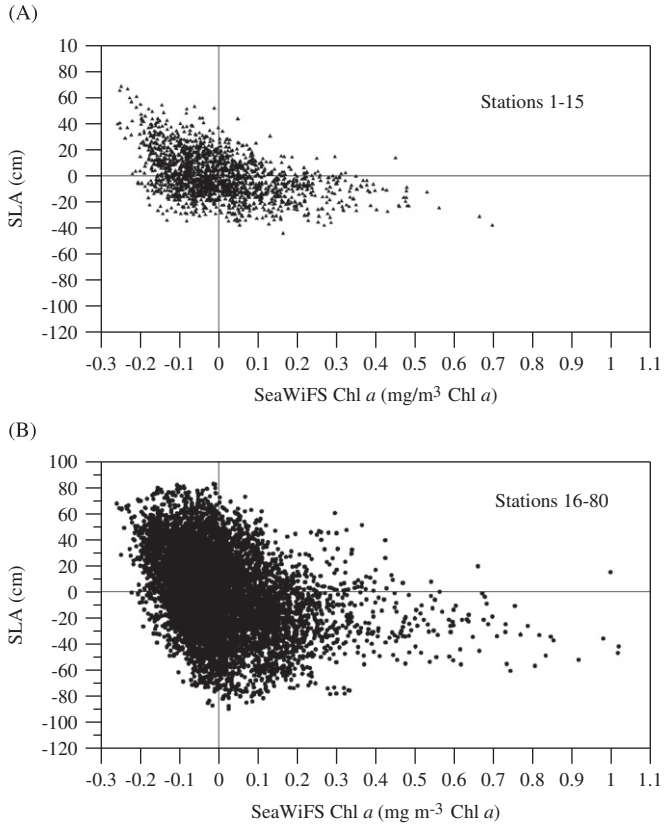

Fig. 12. Correlation between Chl-*a* and SLA residuals along the route of the Kuroshio Extension for (A) stations 1–15 and (B) stations 16–80.

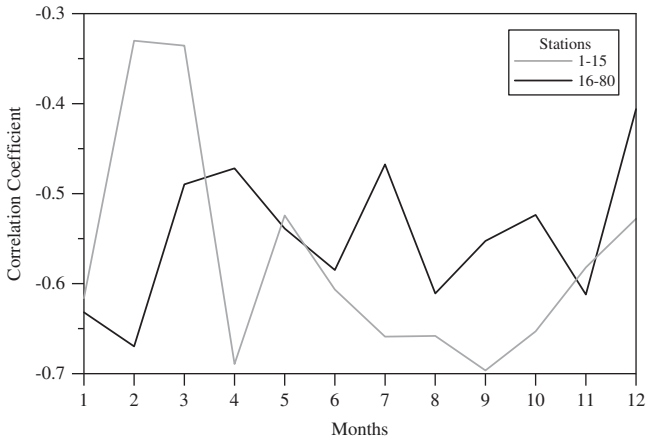

Fig. 13. Monthly correlation coefficient between Chl-*a* anomalies and SLA residuals along the route of the Kuroshio Extension. The results for stations 1–15 are in grey and in black for stations 16–80.

chlorophyll maxima and perhaps this is also the case in the cooler water to the north. Several factors are liable to account for discrepancies between deep-water nutrient supply and mean phytoplankton concentrations. Specifically, the primary productivity may be modulated by the supply of micronutrients, particularly iron, which itself may be associated with the East Asian dust storms. Another mechanism operating here is grazing by zooplankton. The latter means that phytoplankton concentrations should not be simply related to productivity. Thus, the idea here is to guard against making sweeping generalizations regarding the productivity of the different types of eddies and water masses as a whole based just on ocean color.

Acknowledgments

We thank the SeaWiFS Project Office for providing high resolution of SeaWiFS data. Altimeter data were received from NASA. This research was funded by the Office of Naval Research.

References

Arístegui, J., Tett, P., Hernández-Guerra, A., Basterretxea, G., Montero, M.F., Wild, K., 1997. The influence of island generated eddies on chlorophyll distribution: a study of mesoscale variation around Gran Canaria. Deep-Sea Research 44, 71–96.

Chu, P.C., Fang, C.L., 2003. Observed Rossby waves in the South China Sea from satellite altimetry data. In: proceedings of SPIE Conference on Remote Sensing of the Ocean and Sea Ice, pp.142–149.

Gilson, J., Roemmich, D., Cornuelle, B., Fu, L.-L., 1998. Relationship of TOPEX/Poseidon altimetric height to steric height and circulation in the North Pacific. Journal of Geophysical Research 103, 27947–27965.

Hitchcock, G.L., Mariano, A.J., Rossby, T., 1993. Mesoscale pigments fields in the Gulf Stream: observations in a meander crest and trough. Journal of Geophysical Research 98, 8425–8445.

Ichikawa, K., Imawaki, S., 1994. Life history of a cyclonic ring detached from the Kuroshio Extension as seen by the Geosat altimeter. Journal of Geophysical Research 99 (C8), 15953–15966.

Leterme, S.C., Pingree, R.D., 2008. The Gulf Stream, rings and North Atlantic eddy structures from remote sensing (Altimeter and SeaWiFS). Journal of Marine Systems 69, 177–190.

Mizuno, K., White, W.B., 1983. Annual and interannual variability in the Kuroshio Current system. Journal of Physical Oceanography 13, 1847–1867.

Niiler, P., Maximenko, P., McWilliams, J.C., 2003. Dynamically balanced absolute sea level of the global ocean derived from near-surface velocity observations. Geophysical Research Letters 30 (22), 2164, doi:10.1029/2003GL018628.

Qiu, B., Chen, S., 2005. Variability of the Kuroshio Extension jet, recirculation gyre and mesoscale eddies on decadal timescales. Journal of Physical Oceanography 35, 2090–2103.

Sasai, Y., Sasaoka, K., Sasaki, H., Ishida, A., 2007. Seasonal and intra-seasonal variability of chlorophyll-a in the North Pacific: model and satellite data. Journal of the Earth Simulator 8 (11), 3–11.

Solomon, H., 1978. Detachment and recombination of a current ring with the Kuroshio. Nature 274, 58–581.

Stammer, D., 1997. Global characteristics of ocean variability from regional TOPEX/POSEIDON altimeter measurements. Journal of Physical Oceanography, 27, 1743–1769.

Sukigara, C., Suga, T., Saino, T., Toyama, K., Yanagimoto, D., Hanawa, K., Shikama, N., 2009. Subsurface primary production in the western subtropical North Pacific as evidence of large diapycnal diffusivity assocaited with the Subtropical Mode Water. Ocean Science Discussions 6, 1717–1734.

Sun, X., Wang, Y., Yuan, Q., 1989. The surface path of the Kuroshio Extension's western sector and the eddies on both sides. Chinese Journal of Oceanology and Limnology 7 (4), 300–311.

Uz, B.M., Yoder, J.A., Osychny, V., 2001. Pumping of nutrients to ocean surface waters by the action of propagating planetary waves. Nature 409, 597–600.